Journal of Marine Research, 69, 463–481, 2011

Secondary toroidal vortices above seamounts

by Valery N. Zyryanov[1]

ABSTRACT

The classical Taylor-Couette flow appears in a homogeneous fluid between two coaxial cylinders rotating with different angular velocities. The stability loss by a Taylor-Couette flow leads to a bifurcation and generation of Taylor toroidal vortices. In this study we consider an analog to this effect in the case of seamounts in a homogeneous ocean on a f-plane. A seamount is approximated by two coaxial cylinders with heights h_1, h_2 standing one upon the other, the lower cylinder having a larger diameter. Taylor-Couette flow forms in a circular area above the ledge as follows from the differential squeezing of background vorticity above topography. The essential difference from the classical Taylor-Couette flow is the additional background rotation. We demonstrate that in this model ocean a current bifurcation in a circular area above a seamount ledge leads to the generation of toroidal vortices, also known as Taylor vortices in Taylor-Couette flows.

1. Introduction

Now it is well known that topographic anticyclonic eddies with vertical axes of rotation are generated above the mountains in the World Ocean. Studies of the eddy generation above local perturbations of the bed relief in a rotating fluid go back to the theoretical work of Proudman (1916), who proved a theorem stating that the nonviscous motion of a fast rotating fluid is independent of the coordinate parallel to the axis of rotation. Seven years later, Taylor (1923) reproduced this situation in an experiment and found a cylindrical vortex to form above a local perturbation of the bed. These studies were not resumed until 1961.

In 1961, Hide (1961) attempted to interpret the Jupiter's Great Red Spot (JGRS) as a Taylor column above a relief perturbation on Jupiter. Note that Hide was the first to use the term "Taylor column" to a topographic eddy. In 1969, Ingersol (1969) studied the JGRS problem in the context of the quasigeostrophic model with low viscosity and obtained a solution with a stagnant zone within the Taylor column. These astrophysical studies gave an impetus to similar studies in oceanography.

In 1972, McCartney (1972) suggested that lee Rossby waves can be generated downstream of a seamount in zonal flows on the β-plane. Hogg in 1973 published an important work, in which he first presented the theory of topographic eddies in a stratified ocean on

1. Water Problems Institute, RAS, 3, Gubkin Str., 119333, Moscow, Russia. ***email: zyryanov@aqua.laser.ru***

the f-plane with a constant Brunt-Väisälä frequency. He showed that under the effect of stratification the cylindrical Taylor column transforms into a conical vortex with an upward-directed vertex. The vortex may not manifest itself on the ocean surface, and an increase in stratification can cause the vertex to sink even deeper.

Huppert (1975) formulated a criterion of the formation of topographic eddy in a stratified flow on the f-plane with constant Brunt-Väisälä frequency. Analogous criterion for an eastward barotropic flow on the β-plane above an axisymmetric bed perturbation was derived by McCartney (1975). Later McCartney (1976) examined the role of β-effect in the topographic eddy generation and showed a Rossby wave wake to form in eastward flows downstream of a seamount. No such wake was found in westward flows.

Huppert and Bryan (1976) numerically modeled the topographic eddy generation in a homogeneous ocean on the f-plane. They obtained an anticyclonic eddy above a seamount and a cyclonic eddy, which initially drifted downstream of the seamount rotating clockwise around the topographic eddy.

Zyryanov (1981) studied the effect of stratification on the structure of topographic eddies on the β-plane in eastward flows. He showed that generation of baroclinic modes of Rossby waves results in an inverse vorticity in the upper oceanic layers and, as a consequence, in formation of an inverse conical eddy with cyclonic rotation above the Taylor-Hogg near-bed anticyclonic cone.

Studies of the effect of mountains on motions in the atmosphere were reviewed by Smith (1979), and in the ocean by Hogg (1980), Roden (1987), Zyryanov (1995, 2006). Effects of seamounts on biological processes were reviewed by Boehlert and Genin (1987). Results of laboratory modeling of topographic eddies were discussed by Baines and Davies (1980). Boyer, *et al*. (1987) modeled the topographic eddies in a stratified fluid in the laboratory.

The discovery of topographic eddies in the World Ocean can be dated to 1967 when the Russian research vessel "*Astronom*" found that large amounts of fish accumulated above a seamount in the Hawaiian Ridge in the Pacific Ocean. Hydrological survey of the area around the seamount revealed a columnar structure of distributions of hydrological, hydrochemical, and biological characteristics, and the map of dynamical topography clearly demonstrated a closed anticyclonic circulation (Darnitskiy, 1980). In 1975, the topographic eddy above Agulhas Plateau was recorded by using neutral-buoyancy buoys (Grundlingh, 1978).

In the years that followed, detailed experimental studies were conducted on Gayot Fieberling and on the chain of adjacent mountains (Roden, 1994; Eriksen, 1991; Kunze and Toole, 1997; Mullineaux and Mills, 1997), and on Gobb mountain in the Pacific (Freeland, 1994).

An important point is that the observations demonstrate an intense vertical mixing above seamounts (e.g., see Fig. 1). The famous polynya above Kashevarov bank in the Sea of Okhotsk, which is never covered by ice, also is evidence of the mixing (Rogachev and Kosolapkin, 1995). This mixing cannot be explained by traditional theory of topographic eddies which states that motion in the eddy is quasi-two-dimensional and the vertical velocities are small.

The aim of this paper is to show that the vertical mixing can be caused by secondary toroidal vortices developing because of instability of the primary topographic eddy. We

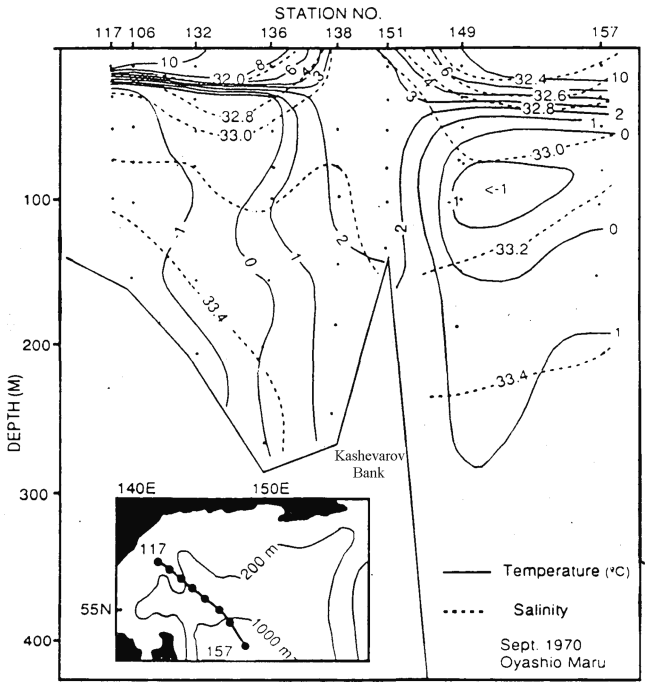

Figure 1. Distributions of temperature and salinity above Kashevarov bank in the Sea of Okhotsk, Sept. 1970 (Kitani and Shimazaki, 1971).

demonstrate for a circular mountain that if the lateral mountain slope has the shape of a ledge, then the velocity field of the primary topographic eddy in the ring domain above the ledge is the same as in the classical Taylor-Couette flow between two rotating cylinders. It is well known that this flow can be unstable in some range of its parameters, the growing perturbations being able to develop into toroidal secondary vortices with axes coinciding with the axis of primary eddy (e.g. Yudovich, 1966). We generalize the classical problem to our case when solid lateral walls are absent and the Earth's rotation is present.

2. Formulation of the problem

The classical Taylor-Couette flow forms in a homogeneous fluid between two coaxial cylinders with radii r_1 and $r_2 (r_1 < r_2)$, rotating with different angular velocities ω_1 (the inner cylinder) and ω_2 (the outer one). Loss of stability by the Taylor-Couette flow leads to a bifurcation and, as a consequence, to generation of Taylor vortices. The radial distribution of the tangential velocity $V_\theta(r)$ is given by the expression

$$V_\theta(r) = ar + \frac{b}{r} \tag{1}$$

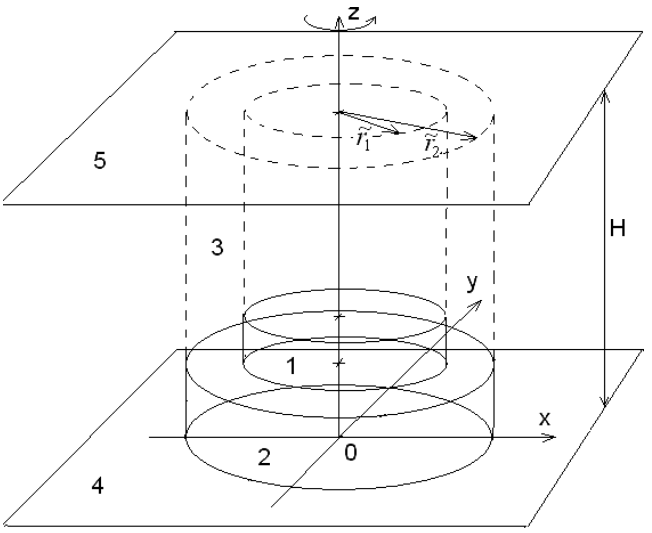

Figure 2. Model seamount in the form of two cylinders; (1) the upper cylinder with a height of $\tilde{h}_1$ and a radius of $\tilde{r}_1$, (2) the lower cylinder with a height of $\tilde{h}_2$ and a radius of $\tilde{r}_2$ ($\tilde{r}_1 < \tilde{r}_2$), (3) the annular region in the fluid above the ledge, (4) sea bottom and (5) surface. The whole system rotates with an angular velocity around the vertical axis z.

where

$$a = \frac{\omega_2 r_2^2 - \omega_1 r_1^2}{r_2^2 - r_1^2}, \quad b = \frac{(\omega_1 - \omega_2) r_1^2 r_2^2}{r_2^2 - r_1^2}. \tag{2}$$

If the cylinders rotate in the positive direction ($\omega_1 > 0, \omega_2 > 0$), then the necessary and sufficient condition for the loss of stability and the generation of secondary torus-like Taylor vortices is

$$\omega_2 r_2^2 - \omega_1 r_1^2 < 0. \tag{3}$$

The classical Taylor-Couette problem was investigated by many authors (Chandrasekhar, 1961; Coles, 1965; Yudovich, 1966; Barkovskiy and Yudovich, 1978); and in stratified fluids by Ermanyuk and Flor (2005) and Guyez *et al.* (2006).

We consider a seamount in a homogeneous ocean on the f-plane approximated by two coaxial cylinders with radii $\tilde{r}_1, \tilde{r}_2$ ($\tilde{r}_1 < \tilde{r}_2$) and heights $\tilde{h}_1, \tilde{h}_2$ standing one upon the other with the lower cylinder having a larger diameter (Fig. 2). Let the fluid flow at the seamount with uniform velocity $\tilde{V}$ along an x-axis. It follows from the theory of topographic eddies (Huppert, 1975; Zyryanov, 1995, 2006) that the nondimensional streamfunction over an axisymmetric seamount, $P(r, \varphi)$, is a sum of an axisymmetric topographic vortex $\sigma\Phi(r)$, and a uniform flow $-V'r \sin\varphi$:

$$P(r, \varphi) = -V'r \sin\varphi + \sigma\Phi(r). \tag{4}$$

Here $r = \tilde{r}/L$ and r, φ are the polar coordinates, L is the horizontal scale of motion, P-the pressure coinciding here with the streamfunction, $V' = \tilde{V}/U_0$, U_0 is a characteristic velocity, σ - the topographic parameter (see below). The function $\Phi(r)$ is written in the form (Huppert, 1975):

$$\Phi(r) = -\int_0^r t^{-1} \int_0^t h(\rho)\rho d\rho dt, \tag{5}$$

where $h(\rho)$ - the radial profile of seamount.

In the case of piece-wise cylindrical seamount with ledge (Fig. 2) we have

$$h(r) = h_1(r) + h_2(r), \tag{6}$$

where

$$h_1(r) = \begin{cases} h_1, & r < r_1 \\ 0, & r > r_1 \end{cases}, \quad h_2(r) = \begin{cases} h_2, & r < r_2 \\ 0, & r > r_2 \end{cases} \tag{7}$$

Substituting (6), (7) into (5) we obtain the following expression for the nondimensional azimuthal velocity:

$$v_0(r) = \sigma \frac{d\Phi}{dr} = -\frac{1}{2}\sigma \begin{cases} (h_1 + h_2)r, r < r_1 \\ h_1 r_1^2 \dfrac{1}{r} + h_2 r, r_1 < r < r_2 \\ (h_1 r_1^2 + h_2 r_2^2)\dfrac{1}{r}, r > r_2 \end{cases} \tag{8}$$

One can see that in the circular area $r_1 < r < r_2$ above a seamount, the radial profile of the tangential velocity $v_0(r)$ coincides with the Taylor-Couette dependence (1)

$$v_0(r) = a_1 r + \frac{b_1}{r} \tag{9}$$

where

$$a_1 = -\frac{\sigma h_2}{2}, \quad b_1 = -\frac{\sigma h_1 r_1^2}{2}, \quad \sigma = \frac{h_0}{H \cdot Ro}, \quad Ro = \frac{U_0}{f_0 L},$$
$$r = \tilde{r}/L, \quad r_1 = \tilde{r}_1/L, \quad r_2 = \tilde{r}_2/L, \quad h_1 = \tilde{h}_1/h_0, \quad h_2 = \tilde{h}_2/h_0. \tag{10}$$

Ro is the Rossby number, f_0 is the characteristic value of Coriolis parameter, h_0 is the characteristic seamount height, H is the oceanic depth outside the seamount. The sign minus in (10) shows that the current in $r_1 < r < r_2$ is an anticyclonic one.

The streamfunction field (4) describes the uniform flow $-V'r \sin\varphi$, which interacts with seamount and spins up the topographic vortex $\sigma\Phi(r)$. If at some moment the uniform flow

$-V'r\sin\varphi$ disappears or becomes weak then only the topographically induced axisymmetric eddy remains over the seamount. In what follows, we examine the stability of this anticyclonic topographic vortex.

At $r = r_1$ and $r = r_2$, the tangential velocity $v_0(r)$ takes the values

$$v_0(r_1) = -\frac{\sigma(h_1 + h_2)r_1}{2},\ v_0(r_2) = -\frac{\sigma(h_2 r_2^2 + h_1 r_1^2)}{2r_2}, \tag{11}$$

respectively. The corresponding angular rotation velocities $\omega_i = v_0(r_i)/r_i, i = 1, 2$ are equal to

$$\omega_1 = -\frac{\sigma(h_1 + h_2)}{2}, \quad \omega_2 = -\frac{\sigma(h_1 r_1^2 + h_2 r_2^2)}{2r_2^2}. \tag{12}$$

As seen from (3), the classical secondary Taylor vortices arise only if $\omega_1 > \omega_2$; i.e., the inner cylinder rotates more rapidly. By virtue of (12) $|\omega_1| > |\omega_2|$, therefore, above seamounts the flow field in the domain $r_1 < r < r_2$ is similar to the classical unstable Taylor-Couette flow with the important distinction that in our case the Earth's rotation is present. It readily follows from (3) that an additional general rotation of both cylinders can violate (3). Therefore, the condition (3) cannot be directly applied to our case.

3. Linear problem of stability

We now introduce the cylindrical coordinates (r, θ, z) and consider an axisymmetrical stationary current which is independent of θ. The velocity $\vec{U}' = (u'_r, u'_\theta, u'_z)$ and pressure P' are sought in the form

$$\vec{U}' = \vec{U} + \vec{U}_0, \quad P' = E \cdot P + P_0, \tag{13}$$

where

$$\vec{U}_0 = (0, v_0(r), 0), \quad \frac{dP_0}{dr} = \frac{v_0^2(r)}{r} - f v_0(r), \tag{14}$$

E is the Ekman number (see below), f - Coriolis parameter nondimensioned on f_0.

Substituting (13), (14) into the primitive equations on f-plane [e.g. Kamenkovich, 1977], we arrive at the system of equations

$$\begin{gathered}
\frac{1}{r}\frac{\partial}{\partial r}(r u_r) + \frac{\partial u_z}{\partial z} = 0 \\
\Delta u_r - \frac{u_r}{r^2} - \frac{\partial P}{\partial r} = \frac{1}{E}\left[u_r\frac{\partial u_r}{\partial r} + u_z\frac{\partial u_r}{\partial z} - \frac{u_\theta^2}{r} - \left(\frac{2v_0}{r} + f\right)u_\theta\right] \\
\Delta u_\theta - \frac{u_\theta}{r^2} = \frac{1}{E}\left[u_r\frac{\partial u_\theta}{\partial r} + u_z\frac{\partial u_\theta}{\partial z} + \frac{u_\theta u_r}{r} + \left(\frac{dv_0}{dr} + \frac{v_0}{r} + f\right)u_r\right] \\
\Delta u_z - \frac{\partial P}{\partial z} = \frac{1}{E}\left[u_r\frac{\partial u_z}{\partial r} + u_z\frac{\partial u_z}{\partial z}\right]
\end{gathered} \tag{15}$$

where

$$\Delta = \frac{\partial^2}{\partial r^2} + \frac{1}{r}\frac{\partial}{\partial r} + \frac{\partial^2}{\partial z^2}, \quad E = E_V = E_L, E_V = \frac{A_z}{f_0 H^2}, E_L = \frac{A_L}{f_0 L^2}; \tag{16}$$

E_V, E_L are the vertical and horizontal Ekman numbers, respectively. We suppose that $L \sim \tilde{r}_2 - \tilde{r}_1 \sim 10\,\text{km}$ and $H \sim 1\,\text{km}$ and therefore we can assume E_V and E_L to be equal to each other.

Linearization of (15) gives the following spectral problem

$$\begin{gathered}
\frac{1}{r}\frac{\partial}{\partial r}(r u_r) + \frac{\partial u_z}{\partial z} = 0 \\
\Delta u_r - \frac{u_r}{r^2} - \frac{\partial P}{\partial r} = \lambda\left(\frac{2v_0}{r} + f\right) u_\theta \\
\Delta u_\theta - \frac{u_\theta}{r^2} = \lambda\left(\frac{dv_0}{dr} + \frac{v_0}{r} + f\right) u_r \\
\Delta u_z - \frac{\partial P}{\partial z} = 0,
\end{gathered} \tag{17}$$

where $\lambda = 1/E$ is the eigenvalue.

The eigensolutions to (17) are represented in the form

$$\begin{aligned}
u_r &= u(r)\cos\alpha z, \quad u_\theta = v(r)\cos\alpha z \\
u_z &= w(r)\sin\alpha z, \quad P = q(r)\cos\alpha z,
\end{aligned} \tag{18}$$

where the functions $w(r)$ and $q(r)$ are related to $u(r)$:

$$w(r) = -\frac{1}{\alpha r}\frac{d}{dr}[r u(r)], \quad q(r) = -\frac{1}{\alpha}\left(\frac{d^2}{dr^2} + \frac{1}{r}\frac{d}{dr} - \alpha^2\right) w(r) \equiv \tilde{L} w(r) \tag{19}$$

The vertical velocity u_z vanishes at the bottom $z = 0$ and at the sea surface $z = 1$, therefore $\alpha = k\pi$. Note that the boundary conditions at the seamount are written at the level $z = 0$ because the bottom perturbations are assumed to be small with respect to the total thickness of the fluid.

Substituting (18) into (17) and taking into account (19), we obtain

$$\begin{gathered}
(L - \alpha^2) u(r) - \frac{dq(r)}{dr} = -\lambda S(r) v(r) \\
(L - \alpha^2) v(r) = \lambda G(r) u(r),
\end{gathered} \tag{20}$$

where

$$S(r) = \frac{2v_0}{r} + f, \quad G(r) = \frac{dv_0}{dr} + \frac{v_0}{r} + f, \quad L = \frac{d^2}{dr^2} + \frac{1}{r}\frac{d}{dr} - \frac{1}{r^2}.$$

By using (19) it is easy to verify that

$$\frac{d}{dr}[\tilde{L}w(r)] - (L - \alpha^2)u(r) \equiv \frac{1}{\alpha^2}(L - \alpha^2)^2 u(r) \tag{21}$$

and to rewrite (20) in the form

$$\begin{aligned}(L - \alpha^2)^2 u &= \alpha^2 \lambda S(r) v \\ (L - \alpha^2)v &= \lambda G(r) u.\end{aligned} \tag{22}$$

4. Boundary conditions

Generation of a topographic vortex above a seamount can be considered as consisting of three stages: an initial stage $t < L/U$ when the fluid moves onto the seamount; an intermediate stage $t \sim O(L/U)$, which lasts for several periods in terms of L/U and during which the vortex structure forms; and the final stage with $t \gg L/U$, when the flow becomes steady. As shown by Verron and Le Provost (1985), the flow reaches a steady state at $t \sim 4L/U$. Next, the vortex's lifetime is determined by the spin-up time $T_S \sim 1/(f E_V^{1/2})$. Thus, the circular Taylor-Couette flow exists at least on times $4L/U < t < T_S$. During this period, the vertical Stewartson's viscous internal boundary layers (Stewartson, 1967) arise along circular vertical surfaces at $r = r_1$ and $r = r_2$ from $z = 0$ to $z = 1$. These boundary layers appear because of the vortex discontinuity which takes place at $r = r_1$ and $r = r_2$ as one can see from (8). The thickness of the Stewartson's layer is $\varepsilon \sim O(E^{1/4})$ and for ocean conditions it is about 10 km. Stewartson's boundary layers at $r = r_1$ and $r = r_2$ are recovered at $r_1 < r < r_2$ and therefore we have the viscous problem (15) in the annulus domain $r_1 < r < r_2$.

At the outer boundary of the first Stewartson's layer at $r \sim r_1 - \varepsilon$ and the outer boundary of the second Stewartson's layer at $r \sim r_2 + \varepsilon$, one can assume the velocity perturbations to vanish. Therefore, we may accept the following boundary conditions

$$[u(r) = v(r) = w(r)]|_{r=r_1, r_2} = 0. \tag{23}$$

From the continuity equation in (17) and the expression for $w(r)$ in (19), one obtains that

$$\int_{r_1}^{r_2} u_z r dr = 0, \tag{24}$$

i.e., the water flow through the cross-section of the cylinder area $r_1 < r < r_2$ is zero for any z.

5. Conditions of bifurcation

System (22) was investigated by Yudovich (1966) for $f = 0$. He proved that if $2v_0/r > 0$ and $dv_0/dr + v_0/r < 0$ for $r_1 < r < r_2$, then for any α, excluding some denumerable set,

the eigenvalue problem (22) has the spectrum of positive and simple eigenvalues $0 < \lambda_1 < \lambda_2 < \ldots$ and each λ_i is a point of bifurcation.

We note that $G(r) = 2a_1 + f = G_0 = const$. Therefore, the application of the operator $(L - \alpha^2)^2$ to the second equation (22) reduces (22) to one equation

$$(L - \alpha^2)^3 v = \lambda^2 \alpha^2 G_0 S(r) v. \tag{25}$$

Using the boundary conditions (23) and Eqs. (19) and (22), we write the boundary conditions for the function $v(r)$:

$$v = Lv = \frac{d}{dr}[(L - \alpha^2)v] = 0, \quad r = r_1, r_2. \tag{26}$$

Eq. (25) together with conditions (26) constitute an eigenvalue problem for the function $v(r)$.

Using the results by Yudovich (1966), we formulate the main theorem.

THEOREM. *If the inequality*

$$Q(r) = S(r)G_0 < 0 \tag{27}$$

is satisfied, then given α *the eigenvalue problem (25), (26) has a positive and simple spectrum* $\{\lambda_i\}$.

Taking into account (9), (10) one can show that (27) is valid in two cases:

Case 1: $S(r) > 0$, $G_0 < 0$. This case corresponds to a crater for which

$$h_2 > f/\sigma, \quad h_1 < \frac{r_2^2}{\sigma r_1^2}(f - \sigma h_2) < 0. \tag{28}$$

Case 2: $S(r) < 0$, $G_0 > 0$. This case corresponds to a seamount as in Figure 2 for which

$$h_2 < f/\sigma, \quad h_1 > \frac{r_2^2}{\sigma r_1^2}(f - \sigma h_2) > 0. \tag{29}$$

So, the bifurcation of the Taylor-Couette flow above seamount is possible, if either (28) or (29) are satisfied. In Case 2 one can write

$$\frac{h_0}{H} = h_1 + h_2. \tag{30}$$

Assuming the dimensionless Coriolis parameter f to be unity, we obtain from (10), (30) and the first inequality (29) that

$$h_2(h_1 + h_2) < Ro. \tag{31}$$

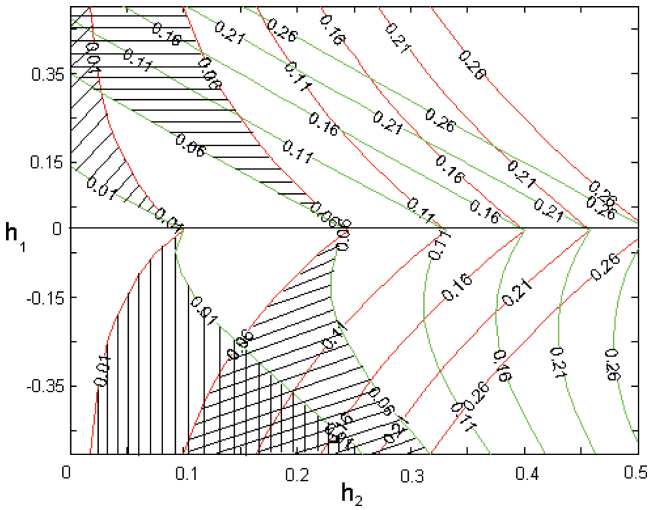

Figure 3. Domains (tongues) of allowable values of cylinder heights h_1 and h_2 depending on the Rossby number Ro for $\delta = r_2/r_1 = 10/7$. The negative values of h_1 refer to the case of a crater.

From the second inequality (29) we have

$$\left(\frac{h_1}{\delta^2} + h_2\right)(h_1 + h_2) > Ro, \tag{32}$$

where $\delta = r_2/r_1$.
Thus by virtue of (31) and (32), the sufficient conditions (29) can be written as

$$h_2(h_1 + h_2) < Ro < \left(\frac{h_1}{\delta^2} + h_2\right)(h_1 + h_2). \tag{33}$$

In Case 1 (a crater) we determine h_0 as

$$\frac{h_0}{H} = |h_1| + h_2, \tag{34}$$

and conditions (28) take the form

$$h_2(|h_1| + h_2) > Ro > \left(\frac{h_1}{\delta^2} + h_2\right)(|h_1| + h_2). \tag{35}$$

Conditions (33), (35) determine domains of allowable values h_1 and h_2 given Rossby number Ro. The domains have the form of tongues (Fig. 3).

6. Spectrum calculation

To calculate the eigenvalues $0 < \lambda_1 < \lambda_2 < \dots$ we represent (25) as the system of ordinary differential equation of sixth order

$$\left.\begin{aligned} \frac{dv_i}{dr} &= v_{i+1}, i = 1, \dots, 5 \\ \frac{dv_6}{dr} &= -\sum_{j=1}^{6} a_j v_j \end{aligned}\right\}, \tag{36}$$

where

$$\begin{aligned} a_1 &= -45/r^6 + 9\alpha^2/r^4 - 3\alpha^4/r^2 - \alpha^6 - \lambda^2\alpha^2 G_0 S(r) \\ a_2 &= 45/r^5 - 9\alpha^2/r^3 + 3\alpha^4/r \\ a_3 &= -27/r^4 + 9\alpha^2/r^2 + 3\alpha^4 \\ a_4 &= 12/r^3 - 6\alpha^2/r \\ a_5 &= -6/r^2 - 3\alpha^2 \\ a_6 &= 3/r. \end{aligned} \tag{37}$$

The boundary conditions (26) in terms of v_i take the form:
at $r = r_1$:

$$\begin{aligned} & v_1(r_1) = 0 \\ & -\left(\frac{1}{r_1^2} + \alpha^2\right) v_1(r_1) + \frac{1}{r_1} v_2(r_1) + v_3(r_1) = 0 \\ & v_4(r_1) + \frac{1}{r_1} v_3(r_1) - \left(\frac{2}{r_1^2} + \alpha^2\right) v_2(r_1) + \frac{2}{r_1^3} v_1(r_1) = 0 \end{aligned} \tag{38}$$

at $r = r_2$:

$$\begin{aligned} & v_1(r_2) = 0 \\ & -\left(\frac{1}{r_2^2} + \alpha^2\right) v_1(r_2) + \frac{1}{r_2} v_2(r_2) + v_3(r_2) = 0 \\ & v_4(r_2) + \frac{1}{r_2} v_3(r_2) - \left(\frac{2}{r_2^2} + \alpha^2\right) v_2(r_2) + \frac{2}{r_2^3} v_1(r_2) = 0. \end{aligned} \tag{39}$$

Solution to (36)–(39) is represented as a sum

$$\vec{V} = \sum_{j=1}^{6} \beta_j \vec{Y}_j(\lambda), \quad \vec{V} = (v_1, v_2, \dots, v_6), \tag{40}$$

where the vectors $\vec{Y}_j = (y_j^{(1)} \dots y_j^{(k)} \dots y_j^{(6)})$ satisfy Eqs. (36) with initial conditions on $r = r_1$

$$\vec{Y}_i|_{r=r_1} = (\dots y_i^{(j)} \dots) = \begin{cases} 0, & j \neq i \\ 1, & j = i \end{cases} \tag{41}$$

and β_j are some coefficient to be determined. One can readily see that $\beta_1 = 0$ by virtue of the first condition (38).

Substituting (40) into (38), (39) gives the following linear system for β_j:

$$A(\lambda) \cdot \begin{pmatrix} \beta_2 \\ \vdots \\ \beta_6 \end{pmatrix} = 0, \tag{42}$$

where the matrix A is

$$A = \begin{pmatrix} 1/r_1 & 1 & 0 & 0 & 0 \\ 2/r_1^2 + \alpha^2 & 1/r_1 & 1 & 0 & 0 \\ a_{31} & . & . & . & a_{35} \\ a_{41} & . & . & . & a_{45} \\ a_{51} & . & . & . & a_{55} \end{pmatrix} \tag{43}$$

and

$$\begin{aligned} a_{3j} &= Y_{j+1}^{(1)}(r_2, \lambda), \\ a_{4j} &= \frac{1}{r_2} Y_{j+1}^{(2)}(r_2, \lambda) + Y_{j+1}^{(3)}(r_2, \lambda), \\ a_{5j} &= Y_{j+1}^{(4)}(r_2, \lambda) + \frac{1}{r_2} Y_{j+1}^{(3)}(r_2, \lambda) - \left(\frac{2}{r_2^2} + \alpha^2 \right) Y_{j+1}^{(2)}(r_2, \lambda), \end{aligned} \tag{44}$$

for $j = 1, \dots, 5$. The homogeneous system (42) has nonzero solution if its determinant is zero:

$$D(\lambda) \equiv \det[A(\lambda)] = 0. \tag{45}$$

Given α the roots λ of Eq. (45) constitute the spectrum of the eigenvalue problem (25), (26). To calculate the roots we find numerically the vectors $\vec{Y}_2(\lambda), \dots, \vec{Y}_6(\lambda)$ for some range of the parameter λ fitting λ in such a way that (45) is satisfied with a high accuracy.

The curve $D(R)$, where $R = \lambda^2$, is shown in Figure 4 for $\alpha = \pi$ and in Figure 5 for $\alpha = 2\pi$. Three values R_1, R_2, R_3 in Figure 4 and two values R_1, R_2 in Figure 5 are the first eigenvalues of spectrum.

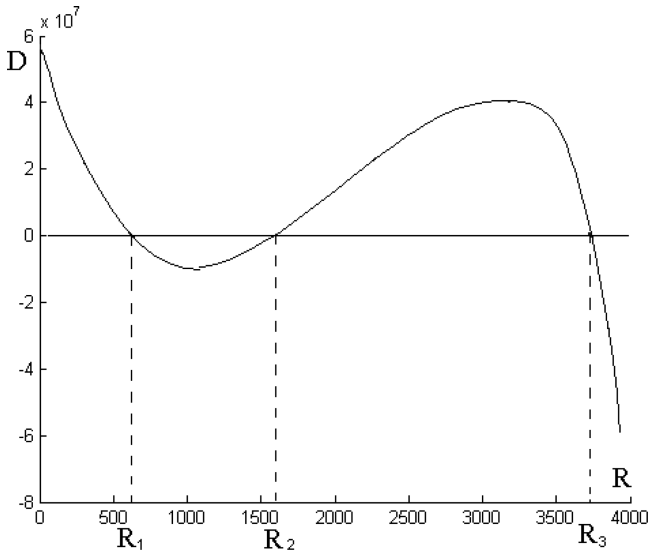

Figure 4. The first three roots R_1, R_2, R_3 of the determinant (45) with $\alpha = \pi$, $h_1 = 0.3$, $h_2 = 0.15$, $\sigma = 5$, $f = 1$, $r_1 = 7$, $r_2 = 10$.

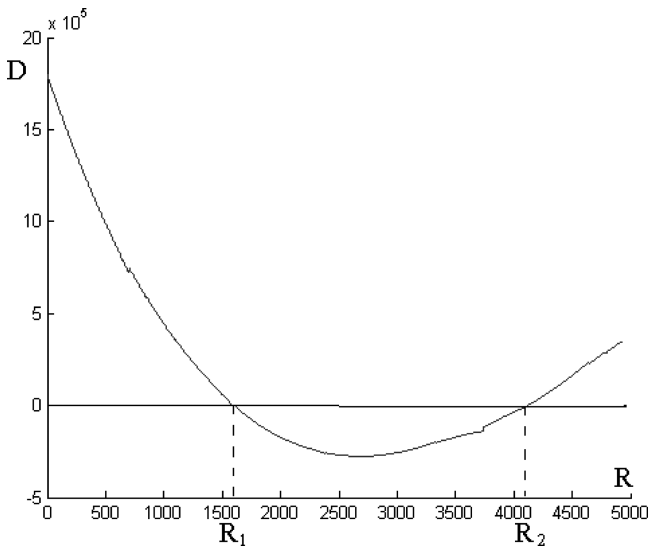

Figure 5. The first two roots R_1, R_2 of the determinant (45) with $\alpha = 2\pi$, $h_1 = 0.3$, $h_2 = 0.15$, $\sigma = 5$, $f = 1$, $r_1 = 3.5$, $r_2 = 5$.

7. Fluid particle trajectories in bifurcation modes

The roots R_1 and R_2 in Figure 4 are $R_1 = 632.292$ and $R_2 = 1592.258$. Consider the case $\lambda_1 = \sqrt{R_1}$. Setting $\beta_2 = 1$ and solving the system of the first four equations (42) we find

$$\beta_3 = -1/7, \beta_4 = -9.89, \beta_5 = 69.78, \beta_6 = -407.72. \tag{46}$$

The corresponding solution of the (25) with boundary conditions (26) has the form

$$v(r) = v_1(r) = \sum_{i=2}^{6} \beta_i Y_i^{(1)}(r). \tag{47}$$

To avoid the errors inherent in the differentiation of discrete numerical solutions and to make the further calculations more convenient, we used a spline approximation of the numerical solution $v(r)$ by 4th order polynomial. Figure 6 represents the behavior of $v(r)$ (solid line) and its spline approximation (dashed line). As one can see from Figure 6, the solution $v(r)$ oscillates on the right end of the area of integration. These oscillations can be either natural or due to computation modes. The answer is still unknown, so further investigations are required.

The spline approximation with $\lambda_1 = \sqrt{R_1}$ is

$$v(r) = 0.0018r^4 + 0.0799r^3 - 2.9781r^2 + 28.6880r - 86.5452 \tag{48}$$

and that with $\lambda_2 = \sqrt{R_2}$ is

$$v(r) = -0.1418r^4 + 5.1216r^3 - 68.7190r^2 + 405.8902r - 890.2810. \tag{49}$$

Substituting (48), (49) into the second equation (20), we find the function $u(r)$ in (18), and then the function $w(r)$ from the first equation (19). These functions are plotted in Figure 6.

Knowing $u(r)$, $v(r)$, $w(r)$ one can find from (18) the radial, tangential and the vertical velocities u_r, u_θ and u_z, respectively. The corresponding trajectories of particles are determined from the system

$$\left.\begin{aligned} \frac{dr}{dt} &= u_r(r, z) \\ r\frac{d\theta}{dt} &= u_\theta(r, z) \\ \frac{dz}{dt} &= u_z(r, z) \end{aligned}\right\}$$

Figure 7 showed the space trajectory of a particle starting from the initial point (7.5, 0, 0.2). As one can see, the particle moves along a torus.

Note that particle trajectories on the vortex tori in Figures 7–9 are constructed in the absence of the main flow (9). In fact, the vortex tori are superimposed onto the main current (9).

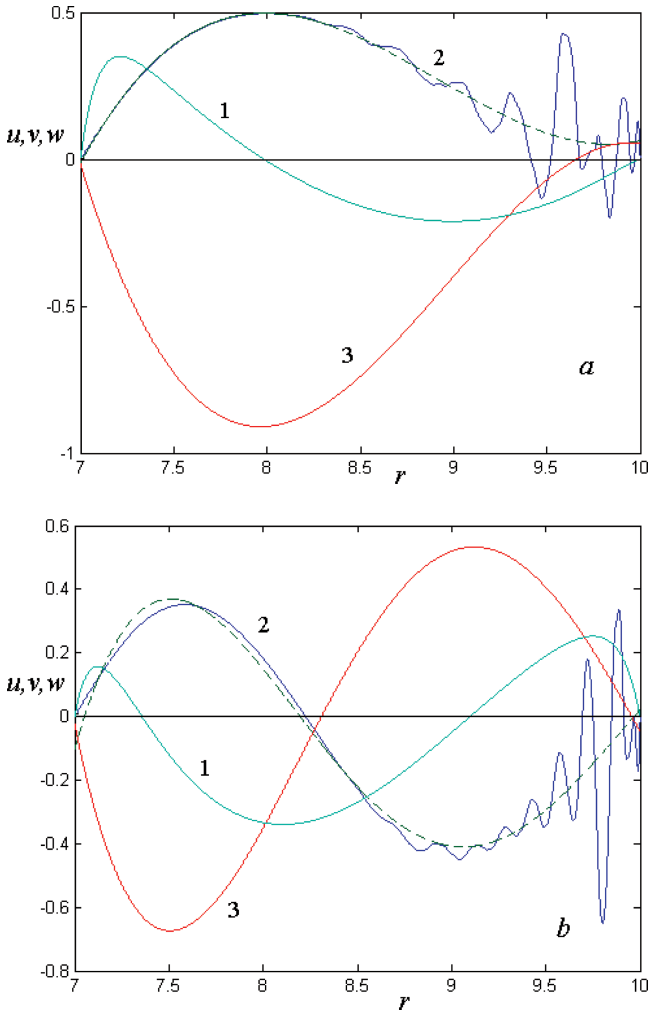

Figure 6. Radial distributions above the ledge of seamount of the functions $w(r)$ (1), $v(r)$, (2: the solid line is the numerical solution (42), the dashed line is the spline approximation), $u(r)$ (3). (a) The first eigenvalue $\lambda_1 = \sqrt{R_1}$; (b) the second eigenvalue $\lambda_2 = \sqrt{R_2}$.

8. Conclusions

The main result of this work is that the bifurcation of Taylor-Couette flow above a ledge of a seamount leads to generation of torus-like circulation and as a consequence, to an intense vertical water exchange above the seamount. According to the classical theory for Taylor-Couette flow (i.e. without external rotation; e.g. Yudovich, 1966), given α one can find Reynolds numbers for which the bifurcation will take place. In the case of Taylor-Couette flow above a seamount the eigenvalues are related to the Ekman numbers whose

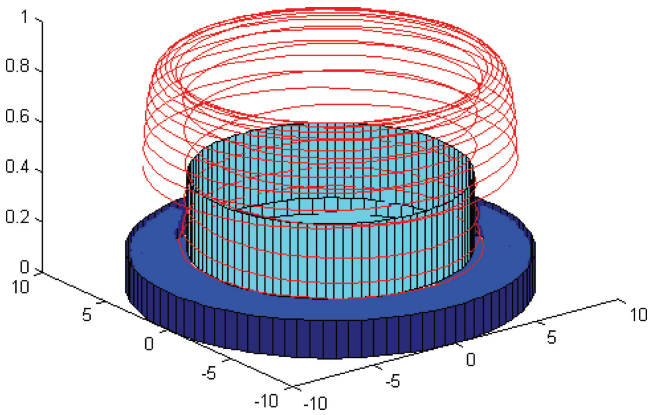

Figure 7. The trajectory of a fluid particle in a topographic eddy with a secondary vortex above the ledge of a seamount in the case of bifurcation at the first eigenvalue $\lambda_1 = \sqrt{R_1}$, $R_1 = 632.29$ for $\alpha = \pi$. The particles rise along a spiral on the inner side of the torus and come down along a spiral on the outer side of the torus.

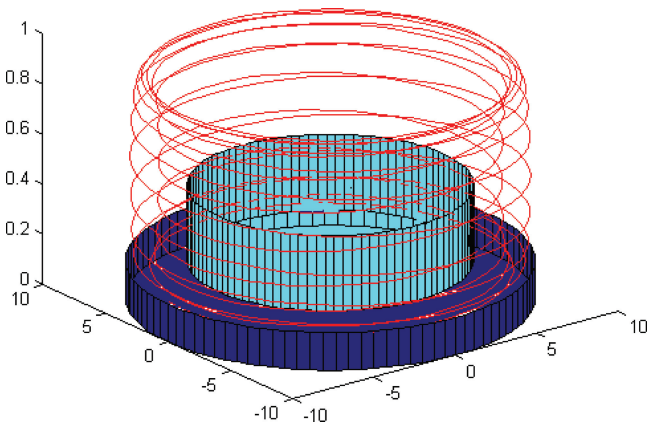

Figure 8. The same as in Figure 7 but for $\lambda_2 = \sqrt{R_2}$, $R_2 = 1592.258$. Contrary to the case of the first eigenvalue (Fig. 7), the particles rise along a spiral on the outer side of the torus and come down along a spiral on the inner side of the torus.

typical values for the ocean are well-known. This means that it is not enough to prove the existence of the spectrum $\{\lambda_i\}$, but one has to calculate this spectrum and to make sure that it corresponds to the real values of Ekman numbers. In the case of the Taylor vortex with one cell we have $R_1 = 632.292$, $R_2 = 1592.257$, that corresponds to $\lambda_1 \cong 25.15$, $\lambda_2 \cong 39.9$ i.e. to the Ekman numbers $E_1 \cong 4 \cdot 10^{-2}$, $E_2 \cong 2.5 \cdot 10^{-2}$. The real oceanic Ekman numbers are somewhat smaller, of the order of $10^{-3} \div 10^{-4}$, and we see from Figures 4, 5 that the values $\lambda = 1/E \approx 10^3 \div 10^4$ are in the spectrum area.

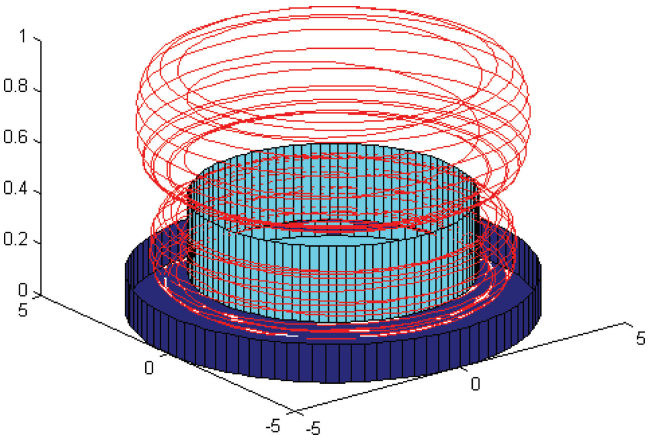

Figure 9. The same as in Figure 7 but for $\alpha = 2\pi$, $\lambda_1 = \sqrt{R_1}$, $R_1 = 1581.4$. Particles move along two tori.

Unfortunately, there are neither direct observations nor laboratory experiments demonstrating existence of toroidal vortices above seamounts. The existence of such vortices can only be supposed based on the intense water mixing above seamounts. One example of water temperature and salinity distributions above Kashevarov Bank in the Sea of Okhotsk was given in Figure 1; similar columns of well-mixed water can be seen above other seamounts in oceans. Thus, strictly speaking, the toroidal vortices in the ocean can be regarded as a theoretical result with indirect confirmations.

As mentioned in Section 4, the turbulent friction contributes largely to the stability loss and formation of vortex tori on times $4L/U < t < T_S$. At the next stage $t \gg T_S$ the vorticity within closed streamlines tends to become a constant because of friction; i.e., the fluid within the vortex tends to rotate as a solid body (Prandtl–Batchelor theorem; Jamagata and Mathuura, 1981). This means that any relative motions of the fluid, including vertical motions and toroidal vortices, should stop and the vortex domain becomes a stagnant zone above a seamount. However, observations of motions above oceanic seamounts give opposite evidence – intense vertical mixing takes place in these domains. Some pumping mechanisms of energy are required to provide this mixing. There are three possible sources of energy: input wind, background current (which spins up the topographic eddy) and residual tidal currents above the seamount. These later are anticyclonic too.

In our model the fluid is assumed homogeneous. The real ocean is always stratified; the effect of water stratification needs further investigations.

Acknowledgments. I thank the referees for their helpful comments. My particular gratitude is addressed to Dr. Gregory Reznik, whose penetrating remarks and thorough scientific editing have contributed appreciably to the improvement of this manuscript. This investigation was supported by the Russian Foundation for Basic Researches, Project 10-05-00432.

REFERENCES

Baines, P. G. and P. A. Davies. 1980. Laboratory studies of topographic effects in rotating and/or stratified flows, *in* Orographic Effects in Planetary Flows, GARP Publication Series, *23*. World Meteorological Organization, Geneva, 235–299.

Barkovskiy, Yu. S. and V. I. Yudovich. 1978. Birth of Taylor eddies in the case of different-rotating cylinders and spectral characteristics of one class of boundary value problems. Reports of Academy of Sciences USSR, *242*, 784–787.

Boehlert, G. W. and A. Genin. 1987. A review of the effect of seamounts on biological processes, *in* Seamounts, Islands and Atolls, Geophys. Monogr. Ser., AGU, Washington DC, 319–334.

Boyer, D. L., P. A. Davies, W. R. Holland, F. Biolley and H. Honji. 1987. Stratified rotating flow over and around isolated three-dimensional topography. Phil. Trans. R. Soc. Lond., *A322*, 213–241.

Chandrasekhar, S. 1961. Hydrodynamic and Hydromagnetic Stability, Dover, 652 pp.

Coles, D. 1965. Transition in circular Couette flow. J. Fluid Mech., *21*, 385–425.

Darnitskiy, V. B. 1980. Baroclinic and barotropic topographic vortices in an ocean. Proc. DVNII, Vladivostok, *86*, 51–62.

Eriksen, C. C. 1991. Observation of amplified flows atop a large seamount. J. Geophys. Res., *96*, 15,227–15,236.

Ermanyuk, E. V. and J. B. Flor. 2005. Taylor-Couette flow in a two-layer stratified fluid: instabilities and mixing. Special issue on rotating and stratified fluids, J. B. Flor and D. Boyer, eds. Dyn. Atmos. Ocean, *40*, 57–69.

Freeland, H. 1994. Ocean circulation at and near Gobb seamount. Deep-Sea Res. I, *41*, 1715–1732.

Grundlingh, M. L. 1978. Drift of satellite-tracked buoy in the Southern Agulhas Current and Agulhas Return Current. Deep-Sea Res., *25*, 1209–1224.

Guyez, E., J. B. Flor and E. Hopfinger. 2006. Diapycnal mixing in Taylor-Couette flow. IUTAM Symposium "Hamiltonian dynamics, vortex structures, turbulence," August 25–30, Moscow.

Hide, R. 1961. Origin of Jupiter's Great Red Spot. Nature, *190*, 895–896.

Huppert, H. E. 1975. Some remarks on the initiation of inertial Taylor columns. J. Fluid Mech., *67*, 397–412.

Huppert, H. E. and K. Bryan. 1976. Topographically generated eddies. Deep-Sea Res., *23*, 655–679.

Hogg, N. G. 1973. On the stratified Taylor column. J. Fluid Mech., *58*, 517–537.

—— 1980. Effects of bottom topography on ocean currents, *in* Orographic Effects in Planetary Flows, GARP Publication Series, *23*, World Meteorological Organization, Geneva, 167–205.

Ingersol, A. P. 1969. Inertial columns and Jupiter's Great Red Spot. J. Atmos. Sci., *26*, 744–752.

Jamagata, T. and T. Mathuura. 1981. A generalization of Prandtl-Batchelor theorem for planetary fluid flow in a closed geostrophic contour. J. Meteor. Soc. Japan. Ser. II, *59*, 615–619.

Kamenkovich, V. M. 1977. Fundamentals of Ocean Dynamics, Elsevier Oceanography Ser., *16*, 249 pp.

Kitani, K. and K. Shimazaki. 1971. On the hydrography of the northern part of the Okhotsk Sea in summer. Bull. Fac. Fish. Hokkaido Univ. *12*, 231–242.

Kunze, E. and J. M. Toole. 1997. Tidally driven vorticity, diurnal shear and turbulence atop Fieberling seamount. J. Phys. Oceanogr., *27*, 2665–2693.

McCartney, M. S. 1972. Taylor columns and Rossby waves generated by isolated topographic features on beta-plane. Notes on the 1972 Summer Study Program in Geophysical Fluid Dynamics at the Woods Hole Oceanogr. Inst., WHOI Ref. 60–81.

—— 1975. Inertial Taylor columns on beta-plane. J. Fluid Mech., *68*, 71–96.

—— 1976. The interaction of zonal currents with topography with application to the Southern Ocean. Deep-Sea Res., *23*, 413–427.

Mullineaux, L. S. and S. W. Mills. 1997. A test of the larval retention hypothesis in seamount-generated flows. Deep-Sea Res. I, *44*, 745–770.

Proudman, G. 1916. On the motion of solid body in a liquid possessing fluids. Proc. Roy. Soc., *A92*, 408–430.

Roden, G. I. 1987. Effect of seamounts and seamount chains on circulation and thermohaline structure, *in* Geophys. Monogr. Ser. AGU, Washington, DC, 335–354.

—— 1994. Effects of the Fieberling seamount group upon flow and thermohaline structure in the spring of 1991. J. Geophys. Res., *99*, 9941–9961.

Rogachev, K. A. and G. Yu. Kosolapkin. 1995. Water mixing on Kashevarov bank (the Sea of Okhotsk). Meteorology and Hydrology, *3*, 96–104.

Smith, R. B. 1979. The influence of mountains on the atmosphere. Adv. in Geophys., *21*, 87–230.

Stewartson K. 1967. On slow transverse motion of a sphere through a rotating fluid. J. Fluid Mech., *30*, 357–369.

Taylor, G. I. 1923. Experiments on the motion of solid bodies in rotating fluids. Proc. Roy. Soc., *A104*, 213–233.

Verron, J. and C. Le Provost. 1985. A numerical study of quasigeostrophic flow over isolated topography. J. Fluid Mech., *154*, 231–252.

Yudovich, V. I. 1966. Secondary flows and the instability of a fluid between rotating cylinders. Appl. Math. Mech., *30*, 689–698.

Zyryanov, V. N. 1981. On the theory of Taylor vortices in a stratified ocean. Fizika Atm. Okeana, *17*, 793–800.

—— 1995. Topographic Eddies in Sea Current Dynamics, Moscow, 240 pp.

—— 2006. Topographic eddies in a stratified ocean. Reg. Chaotic Dyn., *11*, 491–521.

Received: *30 December, 2010*; revised: *6 September, 2011*.